NeuroImage 49 (2010) 2947–2957

Contents lists available at ScienceDirect

NeuroImage

journal homepage: www.elsevier.com/locate/ynimg

Multi-graphical analysis of dynamic PET

Yun Zhou [a,*], Weiguo Ye [a], James R. Bra̧šić [a], Dean F. Wong [a,b,c]

[a] The Russell H. Morgan Department of Radiology and Radiological Science, Johns Hopkins University School of Medicine, 601 N. Caroline St., JHOC room 3245, Baltimore, MD 21287-0807, USA
[b] Department of Psychiatry and Behavioral Sciences, School of Medicine, Johns Hopkins University, Baltimore, MD 21287, USA
[c] Solomon H. Snyder Department of Neuroscience, School of Medicine, Johns Hopkins University, Baltimore, MD 21287, USA

ARTICLE INFO

Article history:
Received 14 August 2009
Revised 1 November 2009
Accepted 11 November 2009
Available online 17 November 2009

Keywords:
Gjedde–Patlak plot
Logan plot
Relative equilibrium
RE plot
PET

ABSTRACT

In quantitative dynamic PET studies, graphical analysis methods including the Gjedde–Patlak plot, the Logan plot, and the relative equilibrium-based graphical plot (RE plot) (Zhou Y., Ye W., Bra̧šić J.R., Crabb A.H., Hilton J., Wong D.F. 2009b. A consistent and efficient graphical analysis method to improve the quantification of reversible tracer binding in radioligand receptor dynamic PET studies. Neuroimage 44(3):661–670) are based on the theory of a compartmental model with assumptions on tissue tracer kinetics. If those assumptions are violated, then the resulting estimates may be biased. In this study, a multi-graphical analysis method was developed to characterize the non-relative equilibrium effects on the estimates of total distribution volume (DV_T) from the RE plot. A novel bi-graphical analysis method using the RE plot with the Gjedde–Patlak plot (RE-GP plots) was proposed to estimate DV_T for the quantification of reversible tracer kinetics that may not be at relative equilibrium states during PET study period. The RE-GP plots and the Logan plot were evaluated by 19 [^{11}C]WIN35,428 and 10 [^{11}C]MDL100,907 normal human dynamic PET studies with brain tissue tracer kinetics measured at both region of interest (ROI) and pixel levels. A 2-tissue compartment model (2TCM) was used to fit ROI time activity curves (TACs). By applying multi-graphical plots to the 2TCM fitted ROI TACs which were considered as the noise-free tracer kinetics, the estimates of DV_T from the RE-GP plots, the Logan plot, and the 2TCM fitting were equal to each other. For the measured ROI TACs, there was no significant difference between the estimates of the DV_T from the RE-GP plots and those from 2TCM fitting ($p = 0.77$), but the estimates of the DV_T from the Logan plot were significantly ($p < 0.001$) lower, 2.3% on average, than those from 2TCM fitting. There was a highly linear correlation between the ROI DV_T from the parametric images (Y) and those from the ROI kinetics (X) by using the RE-GP plots ($Y = 1.01X + 0.23$, $R^2 = 0.99$). For the Logan plot, the ROI estimates from the parametric images were 13% to 83% lower than those from ROI kinetics. The computational time for generating parametric images was reduced by 69% on average by the RE-GP plots in contrast to the Logan plot. In conclusion, the bi-graphical analysis method using the RE-GP plots was a reliable, robust and computationally efficient kinetic modeling approach to improve the quantification of dynamic PET.

Introduction

In quantitative dynamic PET studies, compartmental modeling with plasma input is usually considered as the standard approach for a full analysis of tracer kinetics (Carson, 1986; Gunn et al., 2001; Huang et al., 1980, 1986; Huang and Phelps, 1986; Koeppe et al., 1991; Turkheimer et al., 2003). A compartmental model is usually described by a number of differential equations and parameters for the tracer kinetic process *in vivo*. The parameters of a compartmental model are commonly estimated by fitting the model with measured plasma input to the measured tissue time activity curves (TACs) using nonlinear or linear regression. The selection of a specific compartmental model requires the knowledge of *in vivo* tracer biochemical and physiological processes and the evaluation of model fit. By focusing on the macro-parameters of tracer kinetics such as uptake rate constant K_i and total distribution volume (DV_T), the laborious and complicated procedure of the classical compartmental modeling technique can be remarkably simplified by graphical analysis methods using the Gjedde–Patlak plot (Gjedde, 1981; Patlak and Blasberg, 1985; Patlak et al., 1983; Wong et al., 1986) and the Logan plot (Logan et al., 1990). In general, the Gjedde–Patlak plot is used to estimate K_i for irreversible tracer kinetics, and the Logan plot is used to estimate DV_T for reversible tracer kinetics (Logan, 2003). However, due to the limited durations of the PET scans, some slowly reversible tracer kinetics are also considered as approximately irreversible for graphical analysis using Gjedde–Patlak plot, such as [^{18}F]FDG (Huang et al., 1980; Zhou et al., 2002) and [^{11}C]PIB dynamic PET scans (Blomquist et al., 2008; Edison et al., 2009).

* Corresponding author. Fax: +1 410 955 0696.
E-mail address: yunzhou@jhmi.edu (Y. Zhou).

1053-8119/$ – see front matter © 2009 Elsevier Inc. All rights reserved.
doi:10.1016/j.neuroimage.2009.11.028

Due to their simplicity, computational efficiency, and readily apparent visual representation of tracer kinetic behavior, the graphical analysis methods including the Gjedde–Patlak plot and the Logan plot have been widely used to quantify dynamic PET data. The application of the Logan plot is limited by the noise level of tissue tracer concentration. There are noise-induced negative biases in the estimates of DV_T from the Logan plot, and the underestimation is dependent on both the noise level and magnitude of the tissue concentration (Abi-Dargham et al., 2000; Kimura et al., 2007; Slifstein and Laruelle, 2000). Based on the Logan plot, a few numerical methods have been proposed to reduce the noise-induced negative bias but with higher variation in DV_T estimates and higher computational cost (Buchert et al., 2003; Joshi et al., 2008; Varga and Szabo, 2002; Ogden, 2003).

A relative equilibrium-based graphical analysis method was recently proposed to improve the pixelwise quantification of [^{11}C]PIB and [^{11}C]raclopride dynamic PET (Zhou et al., 2009a,b). The graphical analysis method is based on the assumption that the tissue tracer kinetics attain an equilibrium relative to the input function for $t \geq t^*$, and the relative equilibrium-based graphical plot (RE plot) (same as the "New plot" named in Zhou et al., 2009b) attains a straight line for $t \geq t^*$, where the slope of linear portion ($t \geq t^*$) equals the DV_T if plasma input is used. It was shown that the RE plot is a consistent and computationally efficient graphical analysis method to improve pixelwise quantification of reversible tracer binding in radioligand-receptor dynamic PET studies (Zhou et al., 2009b).

For dynamic PET scans with tracers delivered by bolus administration, reversible tissue tracer kinetics may not attain a relative equilibrium state during the period of PET scanning. The violations in the relative equilibrium condition for the RE plot may result in biased estimates, although its plot could attain a straight line for $t \geq t^*$. In this study, a data-driven multi-graphical analysis was used to analyze the non-relative equilibrium effects on the estimates of DV_T from the RE plot. A bi-graphical analysis method using the RE plot with the Gjedde–Patlak plot (RE-GP plots) was proposed to estimate DV_T for the quantification of reversible tracer kinetics that may not be at relative equilibrium states during the PET study period. The RE plot, the RE-GP plots, and the Logan plot were evaluated by 19 [^{11}C]WIN35,428 ([^{11}C]WIN) and 10 [^{11}C]MDL100,907 ([^{11}C]MDL) normal human dynamic PET studies with tissue tracer kinetics measured at both region of interest (ROI) and pixel levels.

Materials and methods

Data-driven multi-graphical analysis for reversible tracer kinetics

The condition for the multi-graphical analysis is that there is t^* such that the following three graphical plots attain linearity for $t \geq t^*$,

$$\text{RE plot}: \frac{\int_0^t C(s)ds}{C_P(t)} = DV_{RE}\frac{\int_0^t C_P(s)ds}{C_P(t)} + \alpha \quad (1)$$

$$\text{Gjedde}-\text{Patlak plot}: \frac{C(t)}{C_P(t)} = K_P\frac{\int_0^t C_P(s)ds}{C_P(t)} + \beta \quad (2)$$

$$\text{Logan plot}: \frac{\int_0^t C(s)ds}{C(t)} = DV_L\frac{\int_0^t C_P(s)ds}{C(t)} + \gamma \quad (3)$$

where $C_P(t)$ is the tracer concentration in plasma from arterial blood sampling, $C(t)$ is the tissue tracer concentration at time t, DV_{RE} and DV_L are the distribution volumes estimated by the slope of the linear portion of the RE plot and the Logan plot, respectively, K_P is the slope of the linear portion of the Gjedde–Patlak plot, and α, β, and γ are the Y intercepts of the line over the linear segments ($t \geq t^*$) for the RE plot, the Gjedde–Patlak plot, and the Logan plot, respectively. Usually, the values of α and γ from the RE plot and the Logan plot are negative, and the value of β is positive.

Note that any one of above three plots can be derived from the other two graphical plots. Specifically, the Logan plot can be derived from the RE-GP plots with simple algebraic operations for $t \geq t^*$.

$$\frac{\int_0^t C(s)ds}{C(t)} = \left(DV_{RE} - \frac{\alpha K_P}{\beta}\right)\frac{\int_0^t C_P(s)ds}{C(t)} + \frac{\alpha}{\beta} \quad (4)$$

Let

$$DV_{RE-GP} = DV_{RE} - \frac{\alpha K_P}{\beta} \quad (5)$$

$$\gamma_{RE-GP} = \frac{\alpha}{\beta} \quad (6)$$

and compare Eq. (4) with Eq. (3), we have $DV_L = DV_{RE\text{-}GP} = DV_{RE} - \alpha K_P/\beta$, and $\gamma = \gamma_{RE\text{-}GP} = \alpha/\beta$, i.e., the DV_L and γ from the Logan plot can be calculated by the slopes and intercepts from the RE-GP plots.

The above derivation is based on the noise-free tracer kinetics similar to the derivations of the Gjedde–Patlak plot (Patlak et al., 1983), the Logan plot (Logan et al., 1990), and the RE plot (Zhou et al., 2009b) from deterministic compartmental models. Therefore, the $DV_{RE\text{-}GP} = DV_L$ if and only if the noise in the tissue tracer kinetics is negligible.

Based on Eq. (5), the DV_T estimated by the RE-GP plots can be decomposed by two components: (1) the first component is contributed by the relative equilibrium component that can be estimated by the RE plot as DV_{RE}, and (2) the second component is contributed by the non-relative equilibrium component DV_{NRE} that can be estimated by the RE-GP plots as $DV_{NRE} = -\alpha K_P/\beta$. The DV_{NRE} is greater than 0 if the tracer clearance from tissue is slow relative to plasma ($K_P > 0$), and less than 0 if the tracer clearance from tissue is fast relative to plasma ($K_P < 0$) for $t \geq t^*$. The DV_{NRE} is zero if and only if $K_P = 0$, i.e., the $DV_{RE} = DV_L$ if and only if the tracer kinetics attains relative equilibrium for $t \geq t^*$.

DV_T images generated by the RE-GP plots

Due to the high noise levels of pixel tracer kinetics, the parametric images of K_P and β generated by the Gjedde–Patlak plot are usually of high statistical variation. In addition, since division is not a stable operation (Lange et al., 1999), the high variance of K_P and β can result in the large error propagation in the pixelwise calculation of DV_T using Eq. (5) that is associated with the division of $-\alpha K_P/\beta$. On the other hand, it has been shown that both the RE plot and the Gjedde–Patlak plot are consistent graphical methods in term of following two characteristics: (1) the statistical expectations of the slope and intercept from graphical plot with given input are independent of the noise of the target tissue concentration measured by PET; and (2) the slope and the intercept from the ROI TAC are identical to those from the parametric images (Zhou et al., 2009b). Therefore, Eq. (7) below was proposed to generate the DV_T images using the RE-GP plots.

$$DV_T = DV_{RE} - \frac{\alpha s K_P}{s\beta} \quad (7)$$

where sK_P and $s\beta$ are obtained by applying a spatial linear smoothing filter to the images of K_P and β. A 2-D spatial smoothing mean filter (square mask window, equal weighting for all pixels) is usually selected for high noise level of dynamic PET images (Zhou et al., 2003).

Applications to human dynamic PET studies

To investigate the effects of non-relative equilibrium tissue tracer kinetics on the estimates of DV_T from the RE plot, [^{11}C]WIN and [^{11}C]MDL dynamic PET studies for brain imaging of healthy volunteers

were collected in this study. There were 19 (6 females, 13 males, age 29.0 ± 7.9 (mean ± standard deviation hereafter) with range of 18 to 47 years) subjects for [^{11}C]WIN PET scans, and 10 subjects (5 female, 5 male, age 33.2 ± 8.2 with range of 21 to 44 years) for [^{11}C]MDL PET scans. While [^{11}C]WIN was used for *in vivo* imaging dopamine transporter density (Cumming et al., 1999; Frost et al., 1993), [^{11}C]MDL was used for imaging serotonin 5-HT$_{2A}$ receptor density (Gründer et al., 1997; Hall et al., 2000; Lundkvist et al., 1996). All dynamic PET scans were performed on a GE Advance scanner. The PET scanning was started immediately after the intravenous bolus tracer injection of 18.4 ± 1.4 mCi (range 15.8 to 21.6 mCi) with high specific activity of 23723.7 ± 45842.3 mCi/μmol (range 3925.7 to 191837.0 mCi/μmol) for [^{11}C]WIN, and 18.2 ± 4.1 mCi (range 12.8 to 20.8 mCi) with high specific activity of 12775.7 ± 14786.9 mCi/μmol (range 2774.0 to 52780.7 mCi/μmol) for [^{11}C]MDL at time of injection. Metabolite-corrected plasma input functions were obtained for each study by arterial blood sampling. Dynamic PET data were collected in 3-D acquisition mode with protocols of 4 × 0.25, 4 × 0.5, 3 × 1, 2 × 2, 5 × 4, 12 × 5 min (total 90 min, 30 frames) for all scans. To minimize head motion during PET scanning, all participants were fitted with thermoplastic face masks for the PET imaging. Ten-minute ^{68}Ge transmission scans acquired in 2-D mode were used for attenuation correction of the emission scans. Dynamic images were reconstructed using filtered back projection with a ramp filter (image size 128 × 128, pixel size 2 × 2 mm^2, slice thickness 4.25 mm), which resulted in a spatial resolution of about 4.5 mm full-width at half-maximum (FWHM) at the center of the field of view. The decay-corrected reconstructed dynamic images were expressed in μCi/mL. Structural magnetic resonance images (MRIs) (124 slices with image matrix 256 × 256, pixel size 0.94 × 0.94 mm^2, slice thickness 1.5 mm) were also obtained with a 1.5 Tesla GE Signa system for each subject. MRIs were co-registered to the mean of all frames' dynamic PET images using SPM2 with mutual information method. Three ROIs of caudate, cerebellum, and putamen for [^{11}C]WIN, and eleven ROIs of caudate, cerebellum, cingulate, occipital, orbital frontal, parietal, prefrontal, putamen, superior frontal, lateral temporal, and thalamus for [^{11}C]MDL were manually drawn on the co-registered MRIs. ROIs defined on MRIs were copied to the dynamic PET images to obtain ROI TACs.

DV$_T$ estimated from ROI kinetics

A two-tissue five-parameter ([K_1, k_2, k_3, k_4, V_P]) compartment model (2TCM) in sequential configuration (Koeppe et al., 1991; Huang et al., 1986; Innis et al., 2007) was used in [^{11}C]WIN and [^{11}C]MDL dynamic PET studies for ROI kinetic modeling (Brownell et al., 1999; Hinz et al., 2007; Ichise et al., 2002; Ito et al., 1998; Watabe et al., 2000; Wong et al., 1993; Zhou et al., 2004), and the cerebellum was identified as the reference tissue for the quantification of [^{11}C]WIN and [^{11}C]MDL specific binding. To reduce the variation of DV$_T$ resulting from the estimates of k_4, a nonlinear model fitting algorithm with k_4 coupled over all ROIs for each dynamic PET study (Cunningham et al., 2004; Zhou et al., 2007) was performed by following three steps. Step1: five parameters ([K_1, k_2, k_3, k_4, V_P]) of the 2TCM model were estimated for all ROI TACs by conventional nonlinear regression with the same initial estimates of ([0.1 0.05 0.01 0.05 0.05]). Step2: The initial estimates for each ROI were updated by the means of estimates over all PET scans, and five parameters of the 2TCM were then re-estimated using the updated initial values for nonlinear regression. Step 3: The estimates from the step 2 were then adjusted by one more nonlinear regression using step 2, but the mean of k_4 estimates from the step 2 over all ROIs of each subject was fixed during nonlinear regression. A Marquardt algorithm (Marquardt, 1963) was used for nonlinear regression to minimize least squares. The DV$_T$ estimated by the 2TCM from ROI TACs was calculated as $(K_1/k_2)(1+k_3/k_4)+V_P$ after model fitting. Akaike Information criterion (AIC) (Akaike, 1976; Turkheimer et al., 2003; Zhou et al., 2007) was calculated after model fitting at Step 2 and model fitting with k_4 coupling (Step 3). The AIC and the percent of coefficient of variation of DV$_T$ estimation were used to evaluate the performance of nonlinear model fitting.

The plot of time t versus $C(t)/C_P(t)$ was used to evaluate the constancy of $C(t)/C_P(t)$ for $t \geq t^*$ for the relative equilibrium condition of tissue kinetics (Zhou et al., 2009b). The RE plot, the Gjedde–Patlak plot, and the Logan plot were applied to all measured ROI TACs with $t^* = 40$ min. To evaluate the noise effects on the estimates from graphical plots, the three graphical plots were also applied to the 2TCM fitted ROI TACs of noise-free tissue tracer kinetics. Eq. (5) was used for the DV$_T$ estimated by the RE-GP plots.

Parametric images generated by the RE-GP plots

The RE plot, the Gjedde–Patlak plot, and the Logan plot were applied to pixelwise kinetics. Eq. (7) was used for the DV$_T$ images to be generated by the RE-GP plots. Two 2-D spatial smoothing filters, one using window size 7 × 7 pixel^2 for [^{11}C]WIN and the other using window size 9 × 9 pixel^2 for [^{11}C]MDL were selected empirically in this study.

The tracer binding potential (BP), an index of reversible specific binding in radioligand receptor PET studies, was calculated as $BP = DV_T/DV_T(\text{cerebellum}) - 1$, where the DV$_T$(cerebellum) is the DV$_T$ of reference tissue (cerebellum) and is used for the DV of free plus nonspecific binding (Huang et al., 1986; Koeppe et al., 1991; Mintun et al., 1984; Innis et al., 2007; Zhou et al., 2009b).

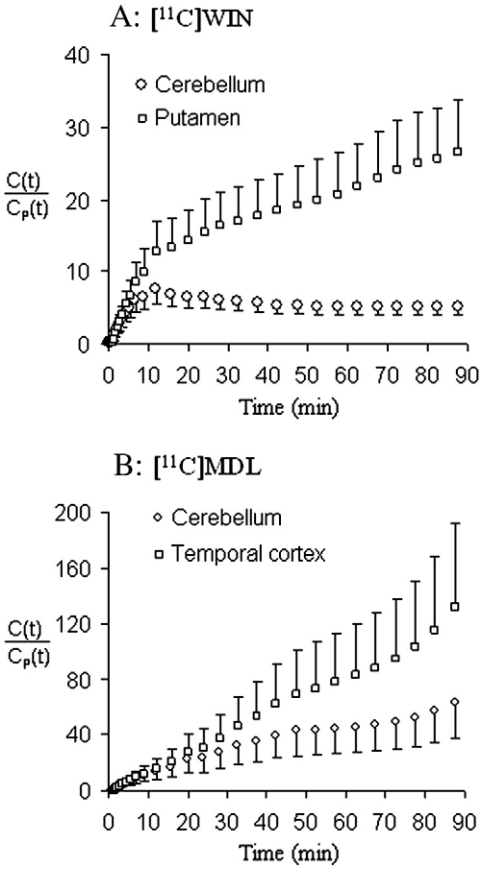

Fig. 1. The mean ± standard deviation of $C(t)/C_P(t)$ as a function of time post tracer injection for [^{11}C]WIN ($n = 19$) (A) and [^{11}C]MDL ($n = 10$) (B). The $C(t)$ is the tissue tracer concentration obtained by applying ROIs to the reconstructed dynamic images, and $C_P(t)$ is the metabolite-corrected tracer concentration in plasma. All plots of mean $C(t)/C_P(t)$ were increasing for $t \geq 42.5$ min except the plot for [^{11}C]WIN cerebellum attained a constant level.

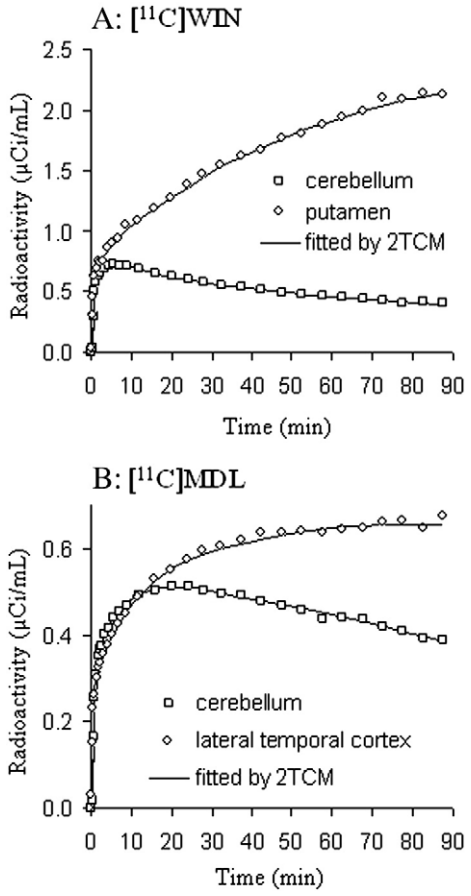

Fig. 2. Typical tissue time activity curves from a [^{11}C]WIN and a [^{11}C]MDL human dynamic PET studies. The fitted curves were obtained by a 2-tissue 5-parameter ([K_1, k_2, k_3, k_4, V_P]) compartment model (2TCM) fitting with plasma input. A nonlinear regression algorithm with k_4 coupled over all ROIs was used for model fitting (see Materials and methods).

Results

Non-relative equilibrium of tissue tracer kinetics

The ratio ($C(t)/C_P(t)$) of the ROI concentration to the plasma input increased as a function of time in all the ROIs in the [^{11}C]MDL studies, but only in the caudate and the putamen in the [^{11}C]WIN studies (Fig. 1). In the [^{11}C]WIN studies the increased rates of the ratio (slope of regression) obtained by linear regression of $C(t)/C_P(t)$ versus t over the later time frame [40 90] were significantly ($p<0.0001$) greater then zero for all the ROIs except for the cerebellum. Note that the cerebellum to plasma input concentration ratio was stable with less than 6% change over the time frame of [40 90] in [^{11}C]WIN studies.

The non-relative equilibrium of tissue tracer kinetics was also shown by the Gjedde–Patlak plot. The positive slope (K_P) of the Patlak plot demonstrated that the $C(t)/C_P(t)$ was increasing as the normalized time $\int C_P(\tau)d\tau/C_P(t)$ increases (see Table 2).

Two-tissue compartment model fitting for ROI kinetics

Paired TACs from two typical studies with fitted kinetics, one from reference tissue (cerebellum) of negligible specific binding, and one from target tissue of high specific binding (putamen for [^{11}C]WIN, lateral temporal cortex for [^{11}C]MDL), were plotted in Fig. 2. All ROI TACs were well fitted consistently by the 2TCM with k_4 coupling. The percent coefficient of variation ($=100\times$standard deviation / mean) of AIC was as low as (8.186 ± 2.185)% ($n=3$) for [^{11}C]WIN and (11.344 ± 2.210)% ($n=11$) for [^{11}C]MDL. In contrast to the AICs from 2TCM model fitting with k_4 coupling, the AICs from the 2TCM without k_4 coupling decreased (-0.076 ± 2.411)% and (0.532 ± 3.925)% for [^{11}C]WIN and [^{11}C]MDL, respectively. The percent reductions in AICs by using the 2TCM model fitting without k_4 coupling were not significant for both [^{11}C]WIN ($p=0.871$) and [^{11}C]MDL ($p=0.248$) studies.

The micro-parameters of ([K_1, k_2, k_3, k_4, V_P]) estimated from ROI TACs using 2TCM model with k_4 coupling and macro-parameter DV_T were listed in Table 1. The percent differences ($=100\times(DV_T$(no k_4 coupling) $-DV_T(k_4$ coupling)) / $DV_T(k_4$ coupling)) between the estimates of [^{11}C]WIN DV_T from ROI TACs using 2TCM fitting without k_4 coupling and those with k_4 coupling were ((-0.173 ± 1.130)%, (0.080 ± 0.581)%, (0.914 ± 1.474)%) for the ROIs of (cerebellum, caudate, putamen). The percent coefficients of variation of [^{11}C]WIN DV_T obtained from ROI TACs of (cerebellum, caudate, putamen) using 2TCM fitting without k_4 coupling were (8.243%, 17.346%, 12.977%) and were similar to those from 2TCM fitting with k_4 coupling (Table 1). However, there were a few outliers in the estimates of [^{11}C]MDL DV_T obtained by 2TCM fitting without k_4 coupling, and the percent differences between the estimates of [^{11}C]MDL DV_T from ROI TACs using 2TCM fitting without k_4 coupling and those with k_4 coupling were ((4.064 ± 5.287)%, (4.540 ± 10.092)%, (0.029 ± 1.490)%, (11.944 ± 34.445)%, (1.843 ± 3.067)%, (0.182 ± 0.955)%, (5.699 ± 16.063)%, (12.155 ± 14.550)%, (0.141 ± 0.746)%, (0.796 ± 1.047)%, (2.479 ± 6.183)%) for the ROIs of (cerebellum, caudate, cingulate, occipital, orbital frontal, parietal, prefrontal, putamen, superior frontal, lateral temporal, and thalamus). The percent coefficient of

Table 1
Estimates (mean (SD)) obtained by fitting a 2-tissue compartment model to ROI kinetics.

ROI	K_1	k_2	k_3	k_4 (coupled among all ROIs)	V_P	DV_T
[^{11}C]WIN35,428 human dynamic PET studies ($n=19$)						
Cerebellum	0.347 (0.039)	0.065 (0.006)	0.007 (0.004)	0.077 (0.030) (range 0.037–0.155)	0.068 (0.021)	5.963 (0.497)
Caudate	0.366 (0.042)	0.077 (0.037)	0.555 (0.179)		0.064 (0.021)	41.868 (7.244)
Putamen	0.400 (0.037)	0.069 (0.097)	0.504 (0.768)		0.073 (0.021)	45.206 (5.517)
[^{11}C]MDL100,907 human dynamic PET studies ($n=10$)						
Cerebellum	0.361 (0.051)	0.041 (0.009)	0.073 (0.033)	0.057 (0.040) (range 0.032–0.162)	0.070 (0.028)	21.210 (2.866)
Caudate	0.401 (0.059)	0.043 (0.022)	0.078 (0.041)		0.079 (0.047)	25.601 (2.974)
Cingulate	0.413 (0.060)	0.041 (0.036)	0.329 (0.304)		0.080 (0.026)	78.496 (13.956)
Occipital	0.365 (0.048)	0.046 (0.032)	0.343 (0.264)		0.057 (0.022)	62.305 (11.975)
Orbital Frontal	0.364 (0.061)	0.035 (0.012)	0.302 (0.199)		0.073 (0.027)	69.189 (14.834)
Parietal	0.362 (0.049)	0.058 (0.070)	0.422 (0.465)		0.060 (0.019)	64.507 (11.947)
Prefrontal	0.367 (0.056)	0.027 (0.012)	0.242 (0.222)		0.065 (0.021)	72.667 (18.177)
Putamen	0.456 (0.058)	0.052 (0.013)	0.093 (0.042)		0.088 (0.046)	24.634 (2.510)
Superior Frontal	0.370 (0.060)	0.037 (0.012)	0.328 (0.182)		0.057 (0.021)	74.066 (17.510)
Lateral Temporal	0.349 (0.053)	0.035 (0.007)	0.382 (0.215)		0.066 (0.017)	81.613 (16.984)
Thalamus	0.418 (0.064)	0.038 (0.016)	0.063 (0.035)		0.078 (0.033)	26.603 (3.390)

variation of [^{11}C]MDL DV_T obtained from ROI TACs using 2TCM fitting without k_4 coupling was reduced (15.0 ± 23.3)% in 11 ROIs with a maximum of 57.0% at occipital cortex by using 2TCM model fitting with k_4 coupling.

The DV_T estimates from ROI TACs using 2TCM fitting with k_4 coupling attained stability when the duration of dynamic PET scan was at least 60 min. There were no significant differences between the estimates of DV_T from 60-min and 90-min dynamic scans with <5% absolute difference.

Graphical plots for ROI kinetic analysis

The RE plot, the Gjedde–Patlak plot, and the Logan plot were applied to each ROI TAC. The multi-graphical plots were evaluated visually and by regular linear regression with statistical analysis. As demonstrated by Fig. 3, all plots generated from ROI kinetics attained linearity in the last 10 points corresponding to the PET scanning time t from 40 to 90 min. The R^2s (mean ± SD) of the linear regression on the linear portion of graphical plots for (RE plot, Gjedde–Patlak plot,

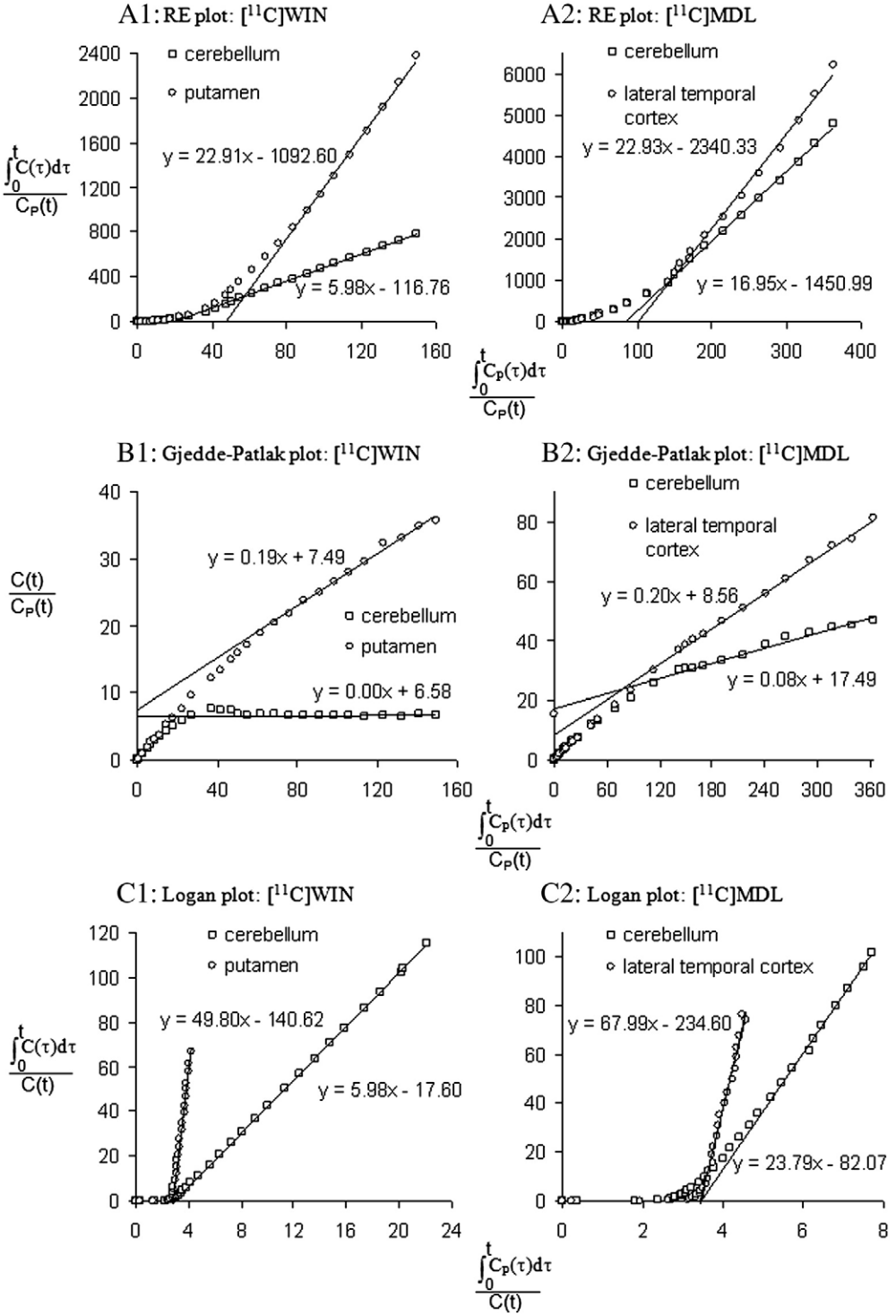

Fig. 3. Multi-graphical plots for the measured typical ROI time activity curves from a [^{11}C]WIN and a [^{11}C]MDL human dynamic PET studies. All plots attained linearity in the last 10 time points that correspond to the time frames from 40 to 90 min post tracer injection.

Logan plot) were (0.998 ± 0.002, 0.813 ± 0.311, 0.986 ± 0.019) ($n = 3 \times 19 = 57$) and (0.979 ± 0.025, 0.884 ± 0.229, 0.987 ± 0.018) ($n = 10 \times 11 = 110$) for [^{11}C]WIN and [^{11}C]MDL, respectively. The linear regression of the Gjedde–Patlak plot showed that the K_Ps for the TACs of caudate and putamen in [^{11}C]WIN and for all cortical ROI TACs in [^{11}C]MDL studies were significantly greater than zero (F-test, $p < 0.001$). The slopes of the linear regression for the Gjedde–Patlak plot from 7 [^{11}C]WIN cerebellum TACs, and 2 [^{11}C]MDL TACs of caudate, putamen, thalamus, cerebellum were not significant different from 0, and R^2s of the linear regression were at relative low values ($R^2 < 0.5$).

The estimates from graphical plots including slope and intercept from the linear regression were summarized in Table 2. In [^{11}C]WIN studies, there were no significant differences (< ±1% difference) between the DVs of cerebellum from the RE plots (DV_{RE}s) and those from the Logan plots (DV_Ls) or the RE-GP plots, because the K_Ps for cerebellum (-0.004 ± 0.010) were not significantly different from 0 (t-test, $p = 0.07$). The [^{11}C]WIN cerebellum kinetics attained relative equilibrium states for t from 40 to 90 min (see Fig. 1). The values of K_P were significantly greater than 0 for caudate and putamen in [^{11}C]WIN, and all 11 ROIs in [^{11}C]MDL studies. Therefore, due to the non-relative equilibrium states in these ROI kinetics, the [^{11}C]WIN DV_{RE} in (caudate, putamen) was lower ((45.9 ± 6.7)%, (46.8 ± 6.2)%), and [^{11}C]MDL DV_{RE} was lower from (19.1 ± 9.2) % at cerebellum to (65.2 ± 6.2) % at lateral temporal cortex, compared to the estimates of DV_T from RE-GP plots.

For the relatively low noise levels of the measured ROI kinetics, the DV_Ts estimated from the Logan plots (DV_L, Table 2) were lower ($p < 0.001$) than those ($DV_{RE\text{-}GP}$s) from the RE-GP plots (Table 2) and those from 2TCM (Table 1). The values of [^{11}C]WIN DV_L in the caudate and the putamen were lower (3.596 ± 4.421)% and (2.887 ± 2.668)% than the DV_Ts from the 2TCM and the RE-GP plots, respectively. The values of [^{11}C]MDL DV_L for all 11 ROIs were (1.952 ± 4.518)% and (2.461 ± 3.373)% lower than the DV_Ts from the 2TCM and the RE-GP plots, respectively. For the measured ROI kinetics, there were no significant differences between the estimates of DV_T from the RE-GP plots and those from 2TCM fitting ($p = 0.77$). There were highly linear correlations between the estimates of DV_T from the RE-GP plots and those from 2TCM or the Logan plot for the measured ROI kinetics (Fig. 4A). The effects of ROI kinetic noise on the DV_T estimates from the graphical plots were demonstrated by Fig. 4A and Fig. 4B. In Fig. 4B, the graphical plots were applied to the fitted ROI TACs for estimating DV_T, where the fitted TACs were obtained by fitting a 2TCM model with k_4 coupling to the measured ROI TACs. With given plasma input function, the 2TCM fitted ROI TACs can be considered as noise-free ROI kinetics. Therefore, the estimates of DV_T from the RE-GP plots were almost identical to those from the 2TCM fitting and those from the Logan plot for the 2TCM fitted ROI TACs (Fig. 4B).

Parametric images generated by graphical plots

One set of representative parametric images generated by the RE plot, the Gjedde–Patlak plot, and the Logan plot from a [^{11}C]WIN and a [^{11}C]MDL dynamic PET studies with MRI images are shown in Fig. 5. The noise levels of parametric images in Fig. 5 were similar through all subject studies for each graphical plot. DV_T images generated by the Logan plot were noisier than DV_T images generated by the RE-GP plots, and the DV_{RE} images were of lowest noise levels. The nonzero pixel values in the K_P images demonstrated the non-relative equilibrium pixel tracer kinetics. The higher K_P pixel values, the higher differences in the pixel values between the DV_Ts generated by the RE-GP plots and the DV_{RE}s from the RE plot. In contrast to the DV_T images generated by the RE-GP plots, the DV_T images generated from the Logan plot demonstrated remarkably lower values with higher noise levels. As the noise of pixel kinetics was increased considerably from the noise level of ROI kinetics, the noise-induced underestimation in the DV_T images generated by the Logan plot was much higher than the underestimation in the DV_T from ROI kinetics as described below.

The DV_T parametric images generated by the RE-GP plots and the Logan plot were compared to those from the ROI kinetics. A highly linear correlation between the DV_Ts from the ROI kinetics and those from the parametric images was obtained with $R^2 = 0.99$ and slope = 1.01 that was not significantly different from 1 ($p = 0.23$) (Fig. 6A). By contrast, a poor linear correlation between the DV_Ts from ROI kinetics and those from parametric images was demonstrated in Fig. 6B for the Logan plot. The poor correlations within each tracer study also resulted from the inconsistencies in the noise-induced underestimation in the DV_T images among the ROIs. The underestimation in the DV_T from the parametric images generated from the [^{11}C]MDL studies was greater than that generated from [^{11}C]WIN studies for the Logan plot. As shown in Fig. 7A, the DV_Ts of (cerebellum, caudate, putamen) from the parametric images were lower (13%, 52%, 50%) than those from ROI kinetics for the Logan plot in [^{11}C]WIN studies. The BPs of (caudate, putamen) from parametric images were lower (50%, 54%) than those from ROI kinetics (Fig. 7B). Similar results for the [^{11}C]MDL studies are shown in Fig. 8. In contrast to the DV_Ts from ROI kinetics, the ROI DV_Ts from parametric images were lower from 36% at cerebellum to 74% at lateral temporal cortex (Fig. 8A); and the BP from parametric images was lower 83% at lateral temporal cortex for the Logan plot (Fig. 8B).

Table 2
Estimates (mean (SD)) from ROI kinetics with graphical plots.

ROI	RE plot		Gjedde–Patlak plot		RE-GP plots	Logan plot	
	DV_{RE}	$-\alpha$	K_P	β	$DV_{RE\text{-}GP}$	DV_L	$-\gamma$
[^{11}C]WIN35,428 human dynamic PET studies ($n = 19$)							
Cerebellum	6.068 (0.535)	133.758 (35.450)	−0.004 (0.010)	7.065 (1.351)	5.986 (0.476)	5.980 (0.478)	18.708 (2.800)
Caudate	21.975 (3.173)	1110.212 (285.886)	0.152 (0.022)	9.044 (2.150)	41.036 (6.532)	39.691 (6.266)	118.454 (19.247)
Putamen	24.212 (3.314)	1217.044 (303.824)	0.170 (0.020)	9.720 (2.264)	45.771 (5.896)	44.607 (5.957)	121.785 (17.258)
[^{11}C]MDL100,907 human dynamic PET studies ($n = 10$)							
Cerebellum	17.306 (2.430)	1699.938 (440.297)	0.056 (0.025)	23.190 (6.412)	21.551 (3.132)	21.486 (3.162)	73.782 (8.000)
Caudate	20.186 (2.933)	2028.418 (519.275)	0.073 (0.028)	25.350 (7.379)	26.334 (3.895)	24.711 (4.131)	71.893 (9.907)
Cingulate	31.688 (5.292)	3699.212 (1008.593)	0.223 (0.045)	18.613 (5.854)	76.894 (12.831)	74.773 (13.490)	195.102 (24.510)
Occipital	26.957 (3.186)	3103.918 (686.460)	0.185 (0.040)	16.686 (3.584)	62.102 (11.946)	61.218 (11.737)	183.897 (20.524)
Orbital Frontal	27.920 (5.481)	3263.843 (966.932)	0.199 (0.045)	15.656 (5.420)	70.470 (13.031)	68.174 (14.269)	203.428 (15.832)
Parietal	27.174 (4.464)	3164.216 (885.125)	0.188 (0.040)	16.707 (5.295)	63.584 (11.308)	62.838 (11.040)	189.749 (20.133)
Prefrontal	28.455 (5.282)	3331.725 (985.927)	0.204 (0.047)	15.619 (4.222)	72.524 (16.399)	71.052 (16.786)	207.568 (21.505)
Putamen	20.512 (2.406)	1985.594 (456.804)	0.067 (0.029)	27.076 (7.095)	25.624 (3.254)	24.954 (3.236)	70.609 (7.454)
Superior Frontal	28.627 (5.657)	3368.900 (1028.899)	0.205 (0.048)	15.814 (4.670)	72.971 (16.875)	71.661 (17.266)	208.378 (21.592)
Lateral Temporal	27.967 (4.820)	3318.133 (957.878)	0.211 (0.044)	13.286 (4.146)	81.858 (16.167)	79.650 (16.920)	244.569 (29.083)
Thalamus	21.056 (2.771)	2096.463 (482.257)	0.070 (0.034)	28.132 (7.658)	26.565 (4.051)	26.006 (3.871)	72.885 (8.201)

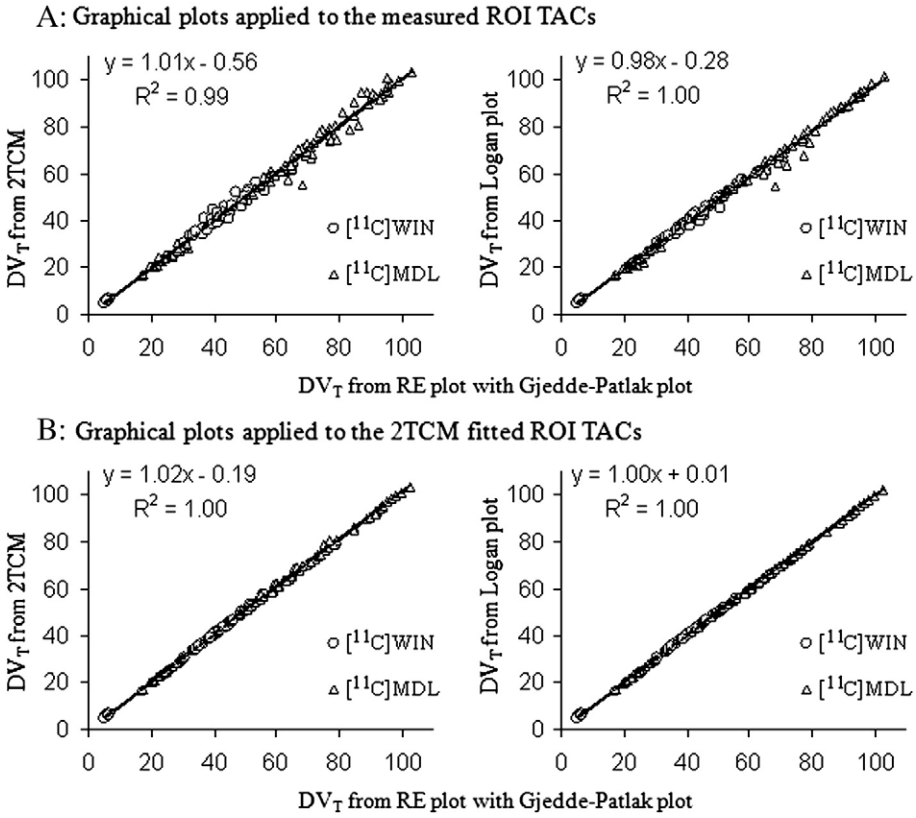

Fig. 4. The linear correlations among the DV_T estimates from multi-graphical plots and those from 2-tissue compartment model (2TCM) fitting with k_4 coupling from 19 [^{11}C]WIN (3 ROIs) and 10 [^{11}C]MDL (11 ROIs) human dynamic PET studies. The DV_T estimates from multi-graphical plots were obtained from the measured (A) and 2TCM fitted ROI time activity curves (TACs) (B). With given plasma input function, the 2TCM fitted ROI TACs can be considered noise as free ROI kinetics, and the measured ROI TACs were used to evaluate the effects of low noise levels on the DV_T estimates from the Logan plot and the RE plot with the Gjedde–Patlak plot (RE-GP plots).

The total computation time for the parametric images generated by the RE-GP plots was 25.3 ± 0.4 s. and 69% less than the time used by the Logan plot. The computational efficiency of the RE-GP plots will be significant for the large volume of dynamic PET data and parametric image estimation in sinogram space (Rahmim et al., 2009).

Discussion

Conditions for the Logan plot and the RE-GP plots

The Logan plot, the RE plot, and the RE-GP plots are mainly used for the quantification of reversible tracer binding. In this study it was

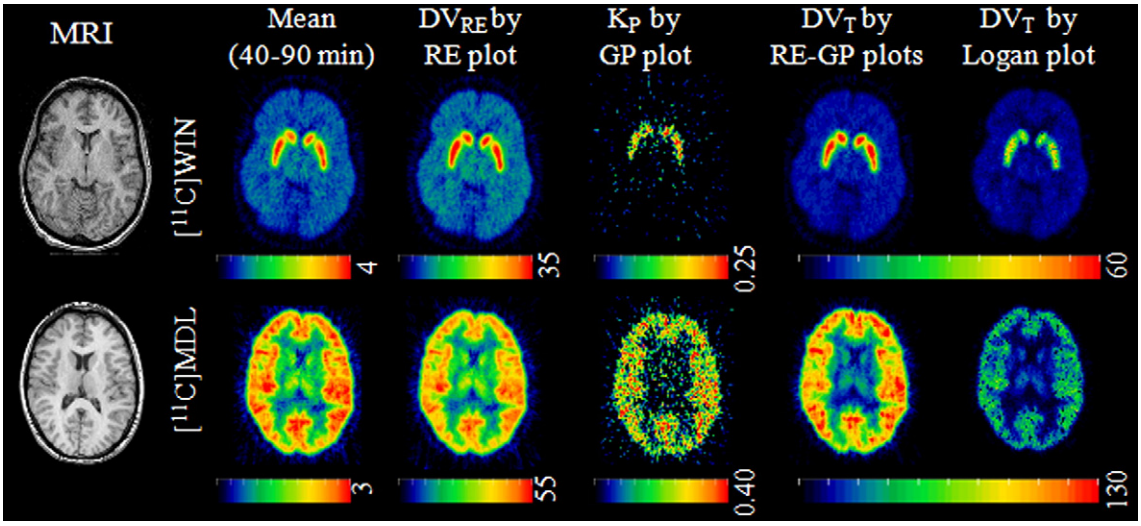

Fig. 5. Transverse parametric images generated by multi-graphical plots in a representative human [^{11}C]WIN and [^{11}C]MDL dynamic PET studies. The MRI and mean images were displayed for reference purpose. The DV_T images generated by the Logan plot were of higher noise level and significantly lower than those from the RE plot with the Gjedde–Patlak plot (RE-GP plots). Due to the noise-induced inconsistent underestimation in the DV_T estimates, the contrast of the DV_T images generated by the Logan plot were markedly decreased. The non-relative equilibrium tracer kinetics was demonstrated by the K_P images from the Gjedde–Patlak plot. The underestimation of DV_T in the DV_{RE} images generated by the RE plot was resulted from non-relative equilibrium tracer kinetics observed in both [^{11}C]WIN and [^{11}C]MDL studies. The mean and DV images were displayed in μCi/mL and mL/mL units, respectively.

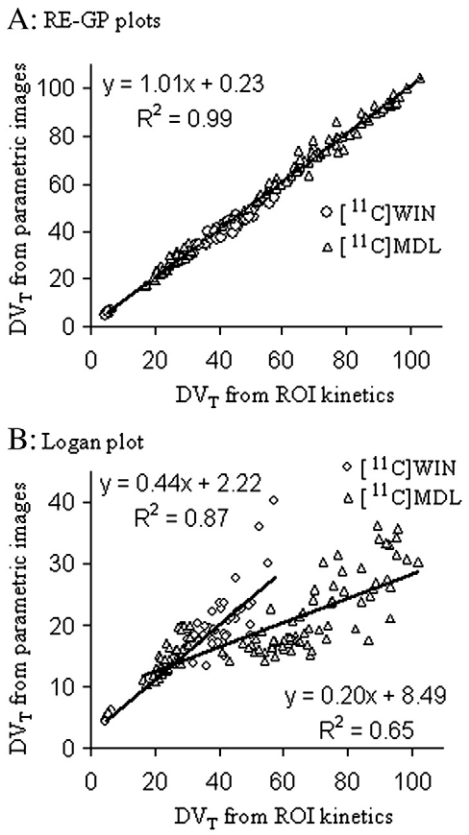

Fig. 6. For the RE plot with the Gjedde–Patlak plot (RE-GP plots) (A), there were high linear correlations between the ROI DV_Ts from the parametric images and those from ROI kinetics. The slope of the linear regression was not significantly different from 1 ($p = 0.23$). Due to the noise-induced inconsistent underestimation in the DV_Ts from the Logan plot, the correlation between the ROI DV_T from parametric images and those from ROI kinetics was poor (B).

shown that tracer total distribution volume DV_T in tissue estimated from the RE plot is unbiased if and only if the tissue tracer kinetics attain equilibrium state relative to plasma input during PET study. Note that the steady state of tissue tracer kinetics is used to derive graphical analysis using the Logan plot with plasma input (Logan et al., 1990), and this condition is stronger than the relative equilibrium condition for the unbiased estimate of DV_T from the RE plot. Due to the apparent inconsistency between theoretical and measured results, it is necessary to re-derive the Logan plot with appropriate conditions assumed on the tracer kinetics, although it was also demonstrated by data and discussed analytically that the steady state of tissue tracer kinetics is not necessary for the Logan plot (Logan et al., 1990; Logan, 2003; Schmidt and Turkheimer, 2002). The sufficient and necessary condition for the distribution volume DV_L obtained by the Logan plot with noise-free tissue kinetics to be an unbiased estimates of total distribution volume DV_T is that there is t^* such that $C(t)$ follows one-tissue compartment model, i.e., for a noise-free tissue kinetics, $DV_L = DV_T$ if and only if there is t^* such that $C(t)$ follows one-tissue compartment model. Different from previous derivations (Logan, 2003; Kimura et al., 2007), the following theoretical proof for the sufficient condition of the Logan plot is based on a general compartment model configuration for reversible tracer kinetics (Logan et al., 1990; Patlak and Blasberg, 1985; Patlak et al., 1983; Zhou et al., 2009a,b). For the sufficient condition, assuming all tissue compartments are reversible and there is t^* such that all tissue compartments attain equilibrium to each other for $t \geq t^*$, i.e., tissue tracer kinetics follow one-tissue compartment model, then the Logan plot attain a linearity for $t \geq t^*$, and the slope of the linear portion equals the DV_T. This can be simply derived as shown below. Based on the integration form of tracer kinetics described by the Eq. (8) (same as Eq. 4 in Zhou et al., 2009b)

$$\int_0^t C(s)ds = \left(-I'K^{-1}Q + V_P\right)\int_0^t C_P(s)ds + I'K^{-1}A(t) \tag{8}$$

where $C_P(t)$ is plasma input function, $A(t) = [C_1(t), C_2(t), \ldots C_m(t)]'$, $C_i(t)$ is the tracer concentration in the ith compartment, $'$ is the mathematical transpose operation, K is the system matrix (mxm) and its elements are the transport rate constants between compartments, Q is a mx1column vector of transport rate constants from vascular space to tissue compartments, I is a mx1 column vector of ones, and V_P is the effective plasma volume in tissue. For the total tissue tracer concentration $C(t)$ measured by PET, we have $C(t) = \Sigma C_i(t) + V_P C_P(t) = I'A(t) + V_P C_P(t)$. Based on the assumption that all tissue compartments attain equilibrium to each other, and $V_P C_P(t)$ is negligible to $C(t)$ for $t \geq t^*$, then we have $C_i(t) = R_i C(t)$, $i = 1, 2, \ldots m$, for $t \geq t^*$, and $I'K^{-1}A(t) = I'K^{-1}RC(t) = \gamma C(t)$, ($\gamma = I'K^{-1}R$ is a constant), where $R = [R_1, \ldots, R_m]'$. In addition, $-I'K^{-1}Q +$

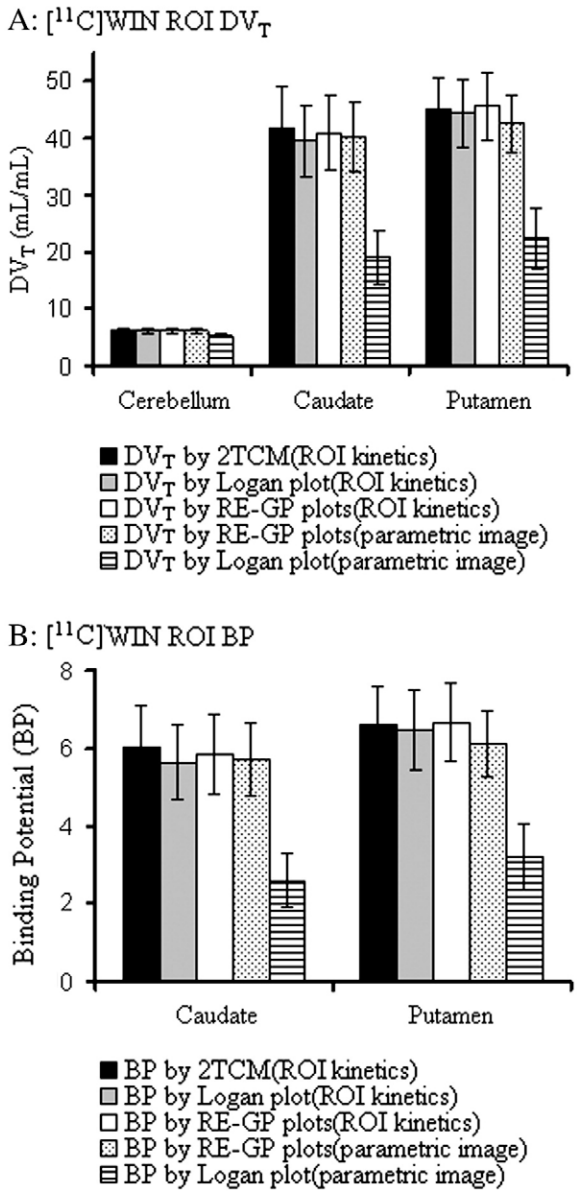

Fig. 7. The mean ± standard error of the ROI DV_Ts (A) and binding potentials (BPs) (B) from 19 [^{11}C]WIN normal human dynamic PET studies. The BP was calculated as DV_T/DV_T(cerebellum) − 1.

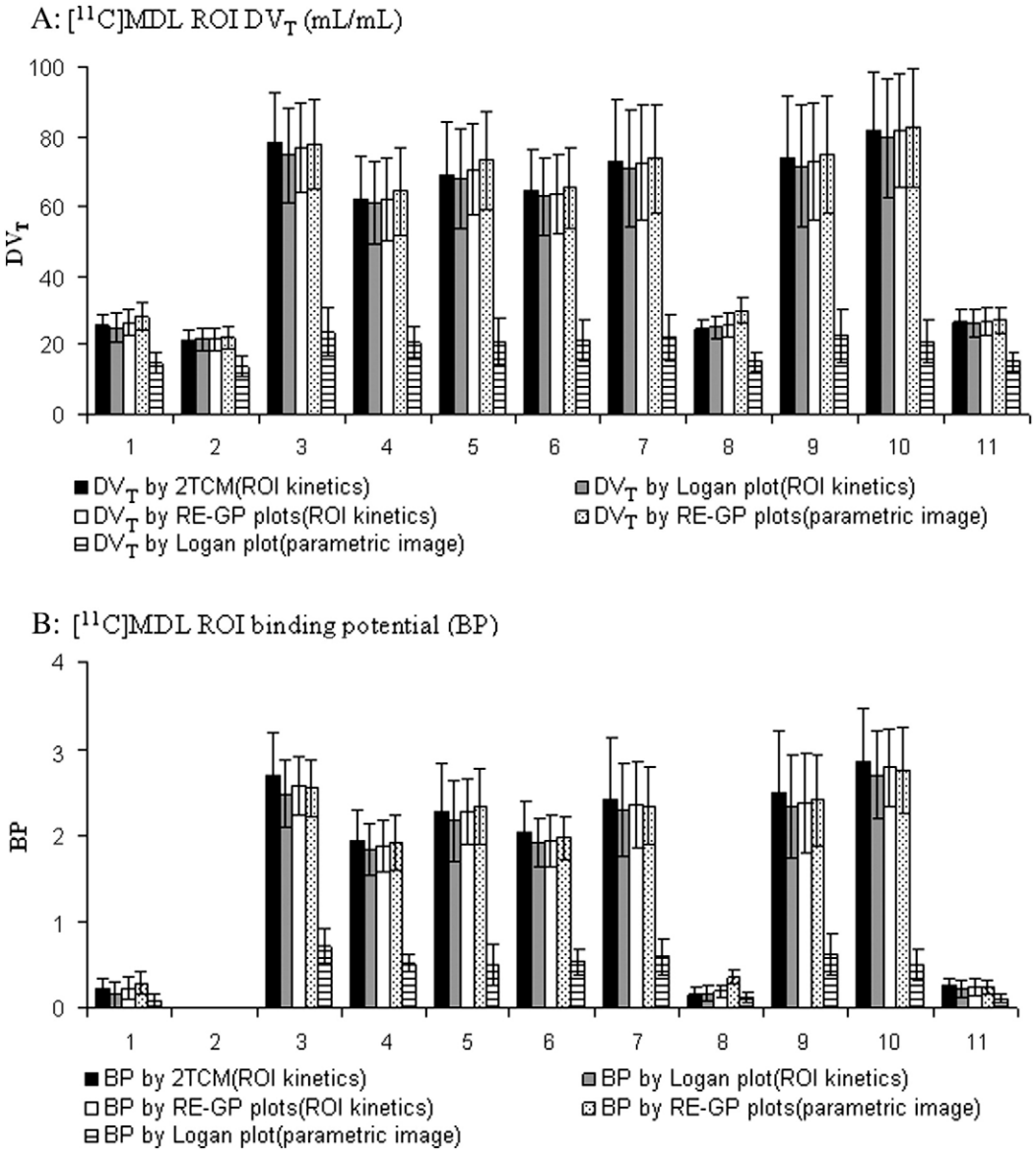

Fig. 8. The mean ± standard error of the ROI DV_Ts (A) and binding potentials (BPs) (B) from 10 [^{11}C]MDL normal human dynamic PET studies. The BP was calculated as DV_T/DV_T(cerebellum) − 1. Regions of interest (ROI) are numbered as: 1: caudate, 2: cerebellum, 3: cingulate, 4: occipital, 5: orbital frontal, 6: parietal, 7: prefrontal, 8: putamen, 9: superior frontal, 10: lateral temporal, 11: thalamus.

$V_P = \Sigma DV_i + V_P = DV_T$, therefore, we have Eq. (9) below that is same as Eq. (3) for the Logan plot for the noise-free tissue kinetics.

$$\int_0^t C(s)ds = DV_T \int_0^t C_P(s)ds + \gamma C(t) \tag{9}$$

This shows that DV_L from the Logan plot equals DV_T. For the necessary condition, it is assumed that the DV_T can be obtained by the Logan plot using Eq. (3). Note that for the noise-free tissue concentration $C(t)$, DV_T and γ obtained by Eq. (3) are identical to those obtained by Eq. (9). Taking derivative on the both sides of Eq. (9), We have Eq. (10) below.

$$\frac{dC(t)}{dt} = \frac{DV_T}{(-\gamma)} C_P(t) - \left(\frac{1}{-\gamma}\right) C(t) \tag{10}$$

The intercept of the linear regression from the Logan plot is usually negative, $DV_T/(-\gamma)$ and $1/(-\gamma)$ in Eq. (10) can be considered as the transport rate constant from plasma to tissue and transport rate constant from tissue to plasma for $t \geq t^*$, respectively. This means that the tissue kinetics follow one-tissue compartment model for $t \geq t^*$.

Based on the necessary and sufficient condition for the Logan plot, if two-tissue compartment model is necessary to describe the tracer kinetics for $t \geq t^*$, then the DV_L form the Logan plot (slope of linear portion of the Logan plot for $t \geq t^*$) could also be a biased estimate of DV_T, although the tracer kinetics is noise-free.

Using the RE-GP plots to quantify reversible tracer binding

In this study, the RE plot was extended to a bi-graphical analysis method using the RE-GP plots to quantify general reversible tracer binding of slow or fast kinetics relative to plasma input. The RE-GP plots are more robust to tracer kinetics than the RE plot for estimating DV_T. It was shown that the estimates of DV_T obtained by the RE-GP plots are identical to those from the Logan plot for tissue tracer kinetics of negligible noise levels. This means that the necessary and sufficient condition for the unbiased estimate of DV_T for the Logan plot is also the basis for the RE-GP plots. However, in contrast to the Logan plot, the estimates of DV_T from the RE-GP plots are more robust to noise levels of tissue tracer kinetics, and reliable for generating parametric images of DV_T. For the low noise and low resolution

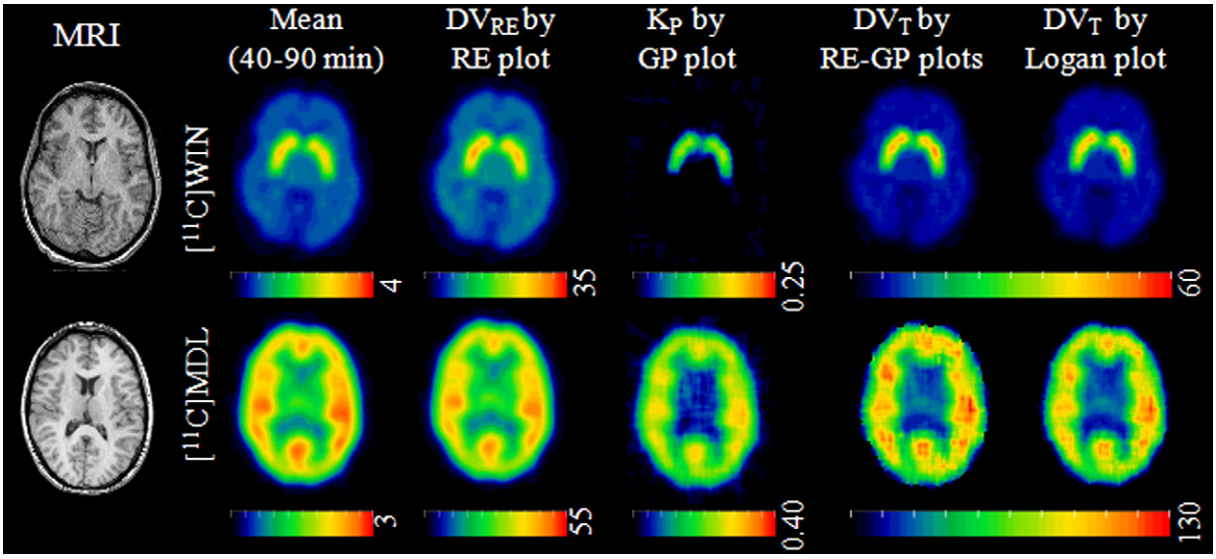

Fig. 9. Transverse parametric images generated by multi-graphical plots in the representative human [^{11}C]WIN and [^{11}C]MDL dynamic PET studies same as those used in the Fig. 5. The MRI and mean images were displayed for reference purpose. Different from the Fig. 5, the mean and parametric images were generated from the spatially smoothed dynamic images, where a 2D mean filter of 7×7 window size and a 2D mean filter of 9×9 window size were used for [^{11}C]WIN and [^{11}C]MDL, respectively. Eq. (5) was used in the RE-GP plots. The mean and DV images were displayed in μCi/mL and mL/mL units, respectively. As the noise levels of pixel kinetics were markedly reduced by applying spatially smooth filter to the dynamic images, the DV_T images generated by the Logan plot were comparable to those generated by the RE-GP plots. The reduced noise-induced underestimation in the DV_T images obtained by the Logan plot is at a high cost of spatial resolution.

dynamic PET images, the DV_T images generated by the Logan plot and RE-GP plots are close to the DV_T images generated by the RE-GP plots, and their main difference is due to the noise-induced underestimation in the Logan plot. Fig. 9 illustrates that the DV_T images generated by the Logan plot and the RE-GP plots are comparable as the DV_T images were generated from the spatially smoothed dynamic images for reducing the noise levels of pixel kinetics, where the two representative PET studies in Fig. 9 are the same as those presented in Fig. 5. Due to low noise levels of the spatially smoothed dynamic PET images, Eq. (5) was used in the RE-GP plots for generation of DV_T images. The resolution of PET images in Fig. 9 was much lower than those in Fig. 5. Due to partial volume effects resulted from spatially smoothing in dynamic images, the ROI values in the DV_T images generated by the RE-GP plots were decreased as high as 29%. In contrast to Fig. 5, the noise-induced underestimation in the DV_T images generated by the Logan plot in Fig. 9 was mostly reduced at the high cost of spatial resolution. In contrast to the ROI values in the DV_T images generated by the RE-GP plots in Fig. 5, the lower ROI values in the DV_T images generated by the Logan plot in Fig. 9 are due to both partial volume effects and noise in pixel kinetics.

For the bi-graphical analysis method using the RE-GP plots, the Gjedde–Patlak (GP) plot is mainly used to estimate the distribution volume contributed from the tracer kinetics not at relative equilibrium states (DV_{NRE}). For example, the K_P from the Gjedde–Patlak plot was recently used as an index to discriminate the patients of Alzheimer's disease from controls using [^{11}C]PIB dynamic PET (Blomquist et al., 2008; Edison et al., 2009). One sufficient condition for the K_P obtained by the Gjedde–Patlak plot to be an unbiased estimate of K_i is that all reversible compartments in tissue attain effective equilibrium (equilibrium relative to tracer plasma kinetics), and there is at least one irreversible compartment in tissue. Previous studies showed that the K_P is a biased estimate of K_i if the reversible compartments are not at relative equilibrium state for $t \geq t^*$ (Yu et al., 1995), or the transport rate constant from the "irreversible" compartments to the reversible compartments are greater than zero (Huang et al., 1980; Patlak and Blasberg, 1985).

In summary, non-relative equilibrium was shown in both [^{11}C]WIN and [^{11}C]MDL kinetics over the usual 90 min PET scan time, and the non-relative equilibrium tracer kinetics resulted in the underestimation of the DV_T from the RE plot, and the non-relative equilibrium induced underestimation can be corrected by a bi-graphical analysis method using the RE-GP plots. The RE, Gjedde–Patlak, and Logan plots were applied to the measured ROI kinetics for the time from 40 to 90 min post tracer injection. The estimates of DV_T from the RE-GP plots were identical to those from the Logan plot for the 2TCM fitted ROIs TACs. For the Logan plot, the ROI estimates from the parametric images were 13% to 83% lower than those from ROI kinetics, and the noise-induced underestimation was dependent on both the noise level of tracer kinetics and the magnitude of DV_T and BP. There was a highly linear correlation between the ROI DV_T from the parametric images (Y) and those from the ROI kinetics (X) by using the RE-GP plots ($Y = 1.01X + 0.23$, $R^2 = 0.99$). The computational time for generating parametric images was reduced by 69% on average by the RE-GP plots in contrast to the Logan plot. In conclusion, the bi-graphical analysis method using the RE-GP plots was a robust and computationally efficient kinetic modeling approach to improve the quantification of noisy dynamic PET data.

Acknowledgments

We thank the cyclotron, PET, and MRI imaging staff of the Johns Hopkins Medical Institutions; Andrew H. Crabb for data transfer and computer administration. This work was supported in part by NIH grants DA00412, MH078175, AA12839, AA012837, and AA10158(DFW). This work was presented in part at the 56th Annual Meeting of the Society of Nuclear Medicine, 2009 in Toronto, Canada (Zhou et al., 2009c).

References

Abi-Dargham, A., Martinez, D., Mawlawi, O., Simpson, N., Hwang, D.R., Slifstein, M., Anjilvel, S., Pidcock, J., Guo, N.N., Lombardo, I., Mann, J.J., Van Heertum, R., Foged, C., Halldin, C., Laruelle, M., 2000. Measurement of striatal and extrastriatal dopamine D1 receptor binding potential with [^{11}C]NNC 112 in humans: validation and reproducibility. J. Cereb. Blood Flow Metab. 20 (2), 225–243.

Akaike, H., 1976. An information criteria (AIC). Math. Sci. 14, 5–9.

Blomquist, G., Engler, H., Nordberg, A., Ringheim, A., Wall, A., Forsberg, A., Estrada, S., Frändberg, P., Antoni, G., Långström, B., 2008. Unidirectional influx and net accumulation of PIB. The Open Neuroimaging J. 2 (2008), 114–125.

Brownell, A.L., Jenkins, B.G., Isacson, O., 1999. Dopamine imaging markers and predictive mathematical models for progressive degeneration in Parkinson's disease. Biomed. Pharmacother. 53 (3), 131–140.

Buchert, R., Wilke, F., van den Hoff, J., Mester, J., 2003. Improved statistical power of the multilinear reference tissue approach to the quantification of neuroreceptor ligandbinding by regularization. J. Cereb. Blood Flow Metab. 23 (5), 612–620.
Carson, R.E., 1986. Parameter estimation in positron emission tomography. In: Phelps, M.E., Mazziotta, J.C., Schelbert, H.R., (Eds.), Positron Emission Tomography and Autoradiography: Principles and Applications for the Brain and Heart. Raven Press, New York, pp. 347–390.
Cumming, P., Yokoi, F., Chen, A., Deep, P., Dagher, A., Reutens, D., Kapczinski, F., Wong, D.F., Gjedde, A., 1999. Pharmacokinetics of radiotracers in human plasma during positron emission tomography. Synapse 34 (2), 124–134.
Edison, P., Brooks, D.J., Turkheimer, F.E., Archer, H.A., Hinz, R., 2009. Strategies for the generation of parametric images of [(11)C]PIB with plasma input functions considering discriminations and reproducibility. NeuroImage 48, 329–338.
Cunningham, V.J., Matthews, J.C., Gunn, R.N., Rabiner, E.A., Gee, A.D., 2004. Identification and interpretation of microparameters in neuroreceptor compartmental models. NeuroImage 22 (Suppl. 2), T13–T14.
Frost, J.J., Rosier, A.J., Reich, S.G., Smith, J.S., Ehlers, M.D., Snyder, S.H., Ravert, H.T., Dannals, R.F., 1993. Positron emission tomographic imaging of the dopamine transporter with 11C-WIN 35,428 reveals marked declines in mild Parkinson's disease. Ann. Neurol. 34 (3), 423–431.
Gjedde, A., 1981. High- and low-affinity transport of D-Glucose from blood to brain. J. Neurochem. 36, 1463–1471.
Gründer, G., Yokoi, F., Offord, S.J., Ravert, H.T., Dannals, R.F., Salzmann, J.K., Szymanski, S., Wilson, P.D., Howard, D.R., Wong, D.F., 1997. Time course of 5-HT2A receptor occupancy in the human brain after a single oral dose of the putative antipsychotic drug MDL 100,907 measured by positron emission tomography. Neuropsychopharmacology 17 (3), 175–185 Erratum in: Neuropsychopharmacology 1998, 19(2):161.
Gunn, R.N., Gunn, S.R., Cunningham, V.J., 2001. Positron emission tomography compartmental models. J. Cereb. Blood Flow Metab. 21, 635–652.
Hall, H., Farde, L., Halldin, C., Lundkvist, C., Sedvall, G., 2000. Autoradiographic localization of 5-HT(2A) receptors in the human brain using [(3)H]M100907 and [(11)C]M100907. Synapse 38 (4), 421–431.
Hinz, R., Bhagwagar, Z., Cowen, P.J., Cunningham, V.J., Grasby, P.M., 2007. Validation of a tracer kinetic model for the quantification of 5-HT(2A) receptors in human brain with [(11)C]MDL 100,907. J. Cereb. Blood Flow Metab. 27 (1), 161–172.
Huang, S.C., Phelps, M.E., 1986. Principles of tracer kinetic modeling in positron emission tomography and autoradiography. In: Phelps, M.E., Mazziotta, J.C., Schelbert, H.R., (Eds.), Positron Emission Tomography and Autoradiography: Principles and Applications for the Brain and Heart. Raven Press, New York, pp. 287–346.
Huang, S.C., Phelps, M.E., Hoffman, E.J., Sideris, K., Selin, C.J., Kuhl, D.E., 1980. Noninvasive determination of local cerebral metabolic rate of glucose in man. Am. J. Physiol. 238, E69–E82
Huang, S.C., Barrio, J.R., Phelps, M.E., 1986. Neuroreceptor assay with positron emission tomography: equilibrium versus dynamic approaches. J. Cereb. Blood Flow Metab. 6 (5), 515–521.
Ito, H, Nyberg, S, Halldin, C, Lundkvist, C, Farde, L., 1998. PET imaging of central 5-HT2A receptors with carbon-11-MDL 100,907. J. Nucl. Med. 39 (1), 208–214.
Ichise, M., Toyama, H., Innis, R.B., Carson, R.E., 2002. Strategies to improve neuroreceptor parameter estimation by linear regression analysis. J. Cereb. Blood Flow Metab. 22 (10), 1271–1281.
Innis, R.B., Cunningham, V.J., Delforge, J., et al., 2007. Consensus nomenclature for *in vivo* imaging of reversibly binding radioligands. J. Cereb. Blood Flow Metab. 27 (9), 1533–1539.
Joshi, A., Fessler, J.A., Koeppe, R.A., 2008. Improving PET receptor binding estimates from Logan plots using principal component analysis. J. Cereb. Blood Flow Metab. 28 (4), 852–865.
Kimura, Y., Naganawa, M., Shidahara, M., Ikoma, Y., Watabe, H., 2007. PET kinetic analysis—pitfalls and a solution for the Logan plot. Ann. Nucl. Med. 21 (1), 1–8.
Koeppe, R.A., Holthoff, V.A., Frey, K.A., Kilbourn, M.R., Kuhl, D.E., 1991. Compartmental analysis of [11C]flumazenil kinetics for the estimation of ligand transport rate and receptor distribution using positron emission tomography. J. Cereb. Blood Flow Metab. 11, 735–744.
Lange, K., 1999. Numerical Analysis for Statisticians. Springer-Verlag, New York.
Logan, J., 2003. A review of graphical methods for tracer studies and strategies to reduce bias. Nucl. Med. Biol. 30 (8), 833–844.
Logan, J., Fowler, J.S., Volkow, N.D., Wolf, A.P., Dewey, S.L., Schlyer, D.J., MacGregor, R.R., Hitzemann, R., Bendriem, B., Gatley, S.J., Christman, D.R., 1990. Graphical analysis of reversible radioligand binding from time-activity measurements applied to [N-11C-methyl]-(-)-cocaine PET studies in human subjects. J. Cereb. Blood Flow Metab. 10, 740–747.
Lundkvist, C., Halldin, C., Ginovart, N., Nyberg, S., Swahn, C.G., Carr, A.A., Brunner, F., Farde, L., 1996. [11C]MDL 100907, a radioligand for selective imaging of 5-HT(2A) receptors with positron emission tomography. Life Sci. 58 (10), 187–192 Erratum in: Life Sci 58(25):379.
Marquardt, D.W., 1963. An algorithm for least-squares estimations of nonlinear parameters. J. Soc. Ind. Appl. Math. 11, 431–441.
Mintun, M.A., Raichle, M.E., Kilbourn, M.R., Wooten, G.F., Welch, M.J., 1984. A quantitative model for the *in vivo* assessment of drug binding sites with positron emission tomography. Ann. Neurol. 15, 217–227.
Ogden, R.T., 2003. Estimation of kinetic parameters in graphical analysis of PET imaging data. Stat. Med. 22 (22), 3557–3568.
Patlak, C.S., Blasberg, R.G., 1985. Graphical evaluation of blood-to-brain transfer constants from multiple-time uptake data. Generalizations. J. Cereb. Blood Flow Metab. 5, 584–590.
Patlak, C.S., Blasberg, R.G., Fenstermacher, J.D., 1983. Graphical evaluation of blood-to-brain transfer constants from multiple-time uptake data. J. Cereb. Blood Flow Metab. 3 (1), 1–7.
Rahmim, A, Zhou, Y, Tang, T., 2009. Direct 4D parametric image estimation in reversible tracer binding imaging. J. Nucl. Med. 50, 137P.
Schmidt, K.C., Turkheimer, F.E., 2002. Kinetic modeling in positron emission tomography. Q. J. Nucl. Med. 46 (1), 70–85 Review.
Slifstein, M., Laruelle, M., 2000. Effects of statistical noise on graphic analysis of PET neuroreceptor studies. J. Nucl. Med. 41, 2083–2088.
Turkheimer, F.E., Hinz, R., Cunningham, V.J., 2003. On the undecidability among kinetic models: from model selection to model averaging. J. Cereb. Blood Flow Metab. 23, 490–498.
Varga, J., Szabo, Z., 2002. Modified regression model for the Logan plot. J. Cereb. Blood Flow Metab. 22 (2), 240–244.
Watabe, H., Channing, M.A., Der, M.G., Adams, H.R., Jagoda, E., Herscovitch, P., Eckelman, W.C., Carson, R.E., 2000. Kinetic analysis of the 5-HT2A ligand [11C]MDL 100,907. J. Cereb. Blood Flow Metab. 20 (6), 899–909.
Wong, D.F., Gjedde, A., Wagner Jr., H.N., 1986. Quantification of neuroreceptors in the living human brain. I. Irreversible binding of ligands. J. Cereb. Blood Flow Metab. 6, 137–146.
Wong, D.F., Yung, B., Dannals, R.F., Shaya, E.K., Ravert, H.T., Chen, C.A., Chan, B., Folio, T., Scheffel, U., Ricaurte, G.A., Neumeyer, J.L., Wagner, H.N., Kuhar, M.J., 1993. In vivo imaging of baboon and human dopamine transporters by positron emission tomography using [11C]WIN 35,428. Synapse 15 (2), 130–142.
Yu, D.C., Huang, S.C., Barrio, J.R., Phelps, M.E., 1995. The assessment of the non-equilibrium effect in the 'Patlak analysis' of Fdopa PET studies. Phys. Med. Biol. 40 (7), 1243–1254.
Zhou, Y., Huang, S.C., Bergsneider, M., Wong, D.F., 2002. Improved parametric image generation using spatial-temporal analysis of dynamic PET studies. NeuroImage 15, 697–707.
Zhou, Y., Endres, C.J., Brašić, J.R., Huang, S.C., Wong, D.F., 2003. Linear regression with spatial constraint to generate parametric images of ligand-receptor dynamic PET studies with a simplified reference tissue model. Neuroimage 18 (4), 975–989.
Zhou, Y., Brašić, J.R., Ye, W., Dogan, A.S., Hilton, J., Singer, H.S., Wong, D.F., 2004. Quantification of cerebral serotonin binding in normal controls and subjects with Tourette's syndrome using [^{11}C]MDL 100,907 and (+)[^{11}C]McN 5652 dynamic PET with parametric imaging approach. NeuroImage 22 (Suppl. 2), T98–T99.
Zhou, Y., Resnick, S.M., Ye, W., Fan, H., Holt, D.P., Klunk, W.E., Mathis, C.A., Dannals, R., Wong, D.F., 2007. Using a reference tissue model with spatial constraint to quantify [^{11}C]Pittsburgh compound B PET for early diagnosis of Alzheimer's disease. Neuroimage 36 (2), 298–312.
Zhou, Y., Resnick, S., Ye, W., Sojkova, J., Wong, D.F., 2009a. Using a consistent graphical analysis method to improve the voxel-wise quantification of [11C]PIB dynamic PET. J. Nucl. Med. 50, 31P.
Zhou, Y., Ye, W., Brašić, J.R., Crabb, A.H., Hilton, J., Wong, D.F., 2009b. A consistent and efficient graphical analysis method to improve the quantification of reversible tracer binding in radioligand receptor dynamic PET studies. NeuroImage 44 (3), 661–670.
Zhou, Y., Ye, W., Brašić, J.R., Wong, D.F., 2009c. Evaluation of a consistent bi-graphical plot to quantify relative slow tracer kinetics in ligand-receptor dynamic PET studies. J. Nucl. Med. 50, 31P.